

Kinetic and Kinematic Sensors-free Approach for Estimation of Continuous Force and Gesture in sEMG Prosthetic Hands^{*}

Gang Liu^{a,b}, Zhenxiang Wang^{b,c}, Chuanmei Xi^{a,b}, Ziyang He^{d,*}, Shanshan Guo^e, Rui Zhang^{a,b,*}, Dezhong Yao^{f,g,*}

^aSchool of Electrical and information Engineering, Zhengzhou University, Zhengzhou(450001), China

^bHenan Key Laboratory of Brain Science and Brain Computer Interface Technology, Zhengzhou University, Zhengzhou(450001), China

^cEngineering Department of International College, Zhengzhou University,450001, China

^dSchool of Cyber Science and Engineering, Zhengzhou University, Zhengzhou(450000), China

^eShanghai Key Laboratory of Brain-Machine Intelligence for Information Behavior, Shanghai International Studies University, City, China

^fClinical Hospital of Chengdu Brain Science Institute, MOE Key Laboratory for NeuroInformation, University of Electronic Science and Technology of China, Chengdu, China

^gResearch Unit of NeuroInformation, Chinese Academy of Medical Sciences, Chengdu, China

Abstract

Regression-based sEMG prosthetic hands are widely used for their ability to provide continuous kinetic and kinematic parameters. However, establishing these models requires complex sensors systems to collect corresponding kinetic and kinematic data in synchronization with sEMG, which is cumbersome and user-unfriendly. This paper proposes a kinetic and kinematic sensors-free approach for controlling sEMG prosthetic hands, enabling continuous decoding and execution of three hand movements: individual finger flexion/extension, multiple finger flexion/extension, and fist opening/closing. This approach utilizes only two data points (-1 and 1), representing maximal finger flexion force label and extension force label respectively, and their corresponding sEMG data to establish a near-linear model based on sEMG data and labels. The model's output labels values are used to control the direction and magnitude of fingers forces, enabling the estimation of continuous gestures. To validate this approach, we conducted offline and online experiments using four models: Dendritic Net (DD), Linear Net (LN), Multi-Layer Perceptron (MLP), and Convolutional Neural Network (CNN). The offline analysis assessed each model's ability to classify finger force direction and interpolate intermediate force values, while online experiments evaluated real-time control performance in controlling gestures and accurately adjusting forces. Our results demonstrate that the DD and LN models provide excellent real-time control of finger forces and gestures, highlighting the practical potential of this sensors-free approach for prosthetic applications. This study significantly reduces the complexity of collecting kinetic and kinematic parameters in sEMG-based regression prosthetics, thus enhancing the usability and convenience of prosthetic hands.

Keywords: Kinetic and kinematic sensor-free, Prosthetic hands, sEMG, Real-time systems

1. Introduction

The motor unit (MU) is the smallest functional unit in the human neuromuscular system, which is composed of motor neurons and innervated muscle fibers [1]. During muscle contraction, a series of motor unit activities produce action potentials that are superimposed on the surface of skin, termed surface electromyography (sEMG) [2, 3]. The sEMG signal reflects the strength of muscle contraction and contains a wealth of information about muscle activity. It is recorded from the skin surface using a portable sensor with some harmless electrodes, so it is a non-invasive, convenient, safe, and painless technique for monitoring muscle contrac-

^{*}This work is supported by the National Natural Science Foundation of China (62303423), the STI 2030-Major Project(2022ZD0208500), Postdoctoral Science Foundation of China (2024T170844,2023M733245), the Henan Province key research and development and promotion of special projects (242102311239), the Shanghai KeyLaboratory of brain-computer Collaborative Information Behavior(2023KFKT005)

^{*}Corresponding authors: Dezhong Yao, Ziyang He, Rui Zhang
Email addresses: gangliu@zzu.edu.cn (Gang Liu), wzx3331@outlook.com (Zhenxiang Wang), 15349896691@163.com (Chuanmei Xi), zyhe@zzu.edu.cn (Ziyang He), guoshanshan@shisu.edu.cn (Shanshan Guo), ruizhang@zzu.edu.cn (Rui Zhang), dyao@uestc.edu.cn (Dezhong Yao)

tion activity [1, 2]. Therefore, the sEMG has the advantages of containing abundant movement and force information, naturalness, low cost, and easy collection. It has been widely applied to in the myoelectric control field, particularly in sEMG prosthesis [4, 5, 6, 7].

Hand amputees face significant challenges in their daily lives, creating a strong demand for intuitive and functional prosthetic solutions. Surface EMG prosthetic hands has emerged as a promising technology for prosthetic control due to its non-invasive nature and ease of use [8]. Current applications of sEMG in prosthetic hands primarily fall into two categories: Classification-based estimation of discrete motion gestures and regression-based estimation of continuous hand joint movements. However, despite the significant potential of sEMG, its practical implementation in prosthetic hands faces several challenges that limit its widespread adoption.

With the rapid development of neural networks in recent years, the deep learning method of classification has been able to realize the recognition of various gestures effectively. Ulysse Côté-Allard et al. have aggregated sEMG data from multiple individuals to propose a classification method based on transfer learning [9]. Zhai, X.L et al. have introduced a self-recalibrating classifier using CNN [10], while Hu, Y et al. have developed an attention-based hybrid CNN-RNN architecture that better captures the temporal characteristics of sEMG signals [11]. However, the scope of application of classification methods is relatively limited, these methods only pay attention to the result of the movement, namely the formed gestures, but ignore the basic composition of the movement such as muscle connectivity to individual fingers force and speed.

To address the limitations of classification-based methods, researchers have explored regression approaches and more general models to decode the fundamental processes of motion from sEMG. While significant progress has been made in predicting joint angles and estimating force and torque, existing methods often rely heavily on kinetic and kinematic sensors for data collection. For instance, studies on finger force estimation, such as those by Hang Su et al. and Gang Liu et al. have developed algorithms and models for human-robot interaction and continuous hand action decoding, respectively [12, 13]. Similarly, Yang Zheng and Xiaogang Hu proposed a neural-driven approach for real-time finger force estimation based on MU discharge events from sEMG [14]. In the area of joint angle prediction, Zhang, Feng et al. employed a simple BP neural network to establish an m th order nonlinear model linking sEMG signals and human leg joint angles [15],

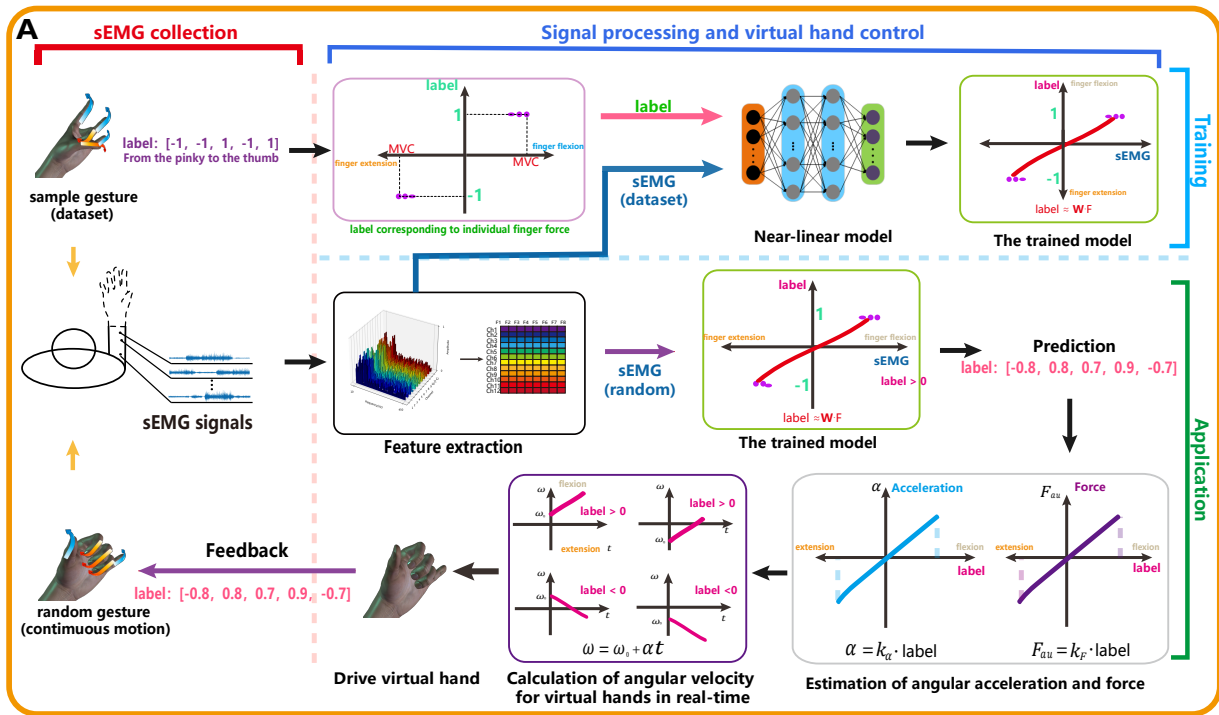
and Ding, Qichuan et al. proposed a state-space motion model with an unscented Kalman filter (UKF) for estimating multi-joint angles from sEMG [16]. Despite these advancements, the reliance on kinetic and kinematic sensors, as highlighted in [17, 18, 19, 20], remains a significant hurdle. Some studies have even utilized 3D motion camera systems system for data collection [21]. This dependence increases system complexity and imposes stringent requirements for synchronized data collection, hindering the development of truly practical and user-friendly sEMG-based prosthetic systems.

This paper introduces a novel kinetic and kinematic sensors-free approach for controlling prosthetic hands. Capitalizing on the near-linear relationship between sEMG amplitude and muscle force within a specific range, our method collects sEMG data at two key points corresponding to maximal finger flexion force and extension force respectively to simulate a continuous range of force values. We define the label for maximal flexion force as 1, and maximal extension force label as -1. To acquire easily recognizable sEMG signals, we specifically choose to collect sEMG data at maximal extension and flexion gestures, which can also acquire maximal force. This data collected is then used to develop a near-linear model based on sEMG and finger force labels for continuous prosthetic finger force control (see Figure 1. Part A: Training). The model’s output labels are then used to accurately decode both the direction and relative magnitude of finger forces, enabling precise gesture control. We establish a linear relationship between the model’s output labels and the actual finger force as follows:

$$F_{au} = k_F \cdot label \quad (1)$$

where F_{au} represents the actual finger force, k_F is a user-specific scaling parameter, and $label$ represents the model’s output (finger force labels). By adjusting the parameter k_F , we can derive the actual finger force and control gestures tailored to individual users. It’s crucial to note that k_F is always positive, solely adjusting the force magnitude. The direction of finger force (flexion or extension) is determined by the positive or negative of the $label$. Therefore, the $label$ can be interpreted as a normalized representation of finger force in positive and negative directions respectively. This approach eliminates the need for complex kinetic and kinematic data acquisition processes, enabling real-time decoding of force magnitude and velocity information, which facilitates more efficient control of prosthetic hands (seen Figure 1. Part A: Application).

The rest of the paper is organized as follows: Section 2 describes the establishment of the model in detail, in-



Data acquisition, training and online application without kinematic sensor

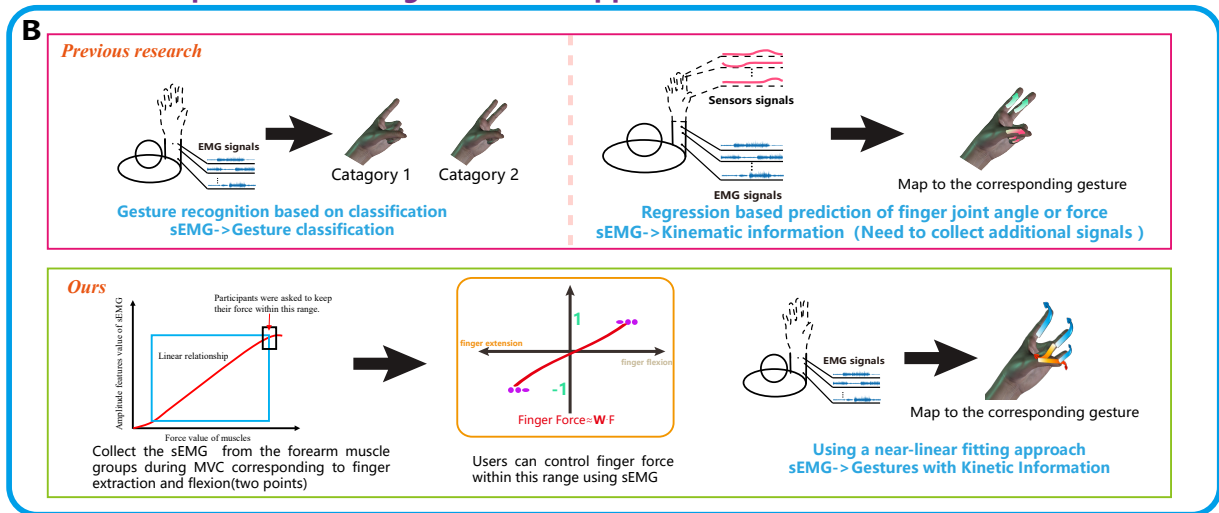


Fig. 1. Continuous prediction of finger force labels and virtual hands control system based on sEMG. Part A demonstrates the process of data acquisition, model training, and online application without the need for kinetic and kinematic sensors. Part B contrasts the differences in methods for gestures recognition and kinetic and kinematic information prediction between this study and previous research.

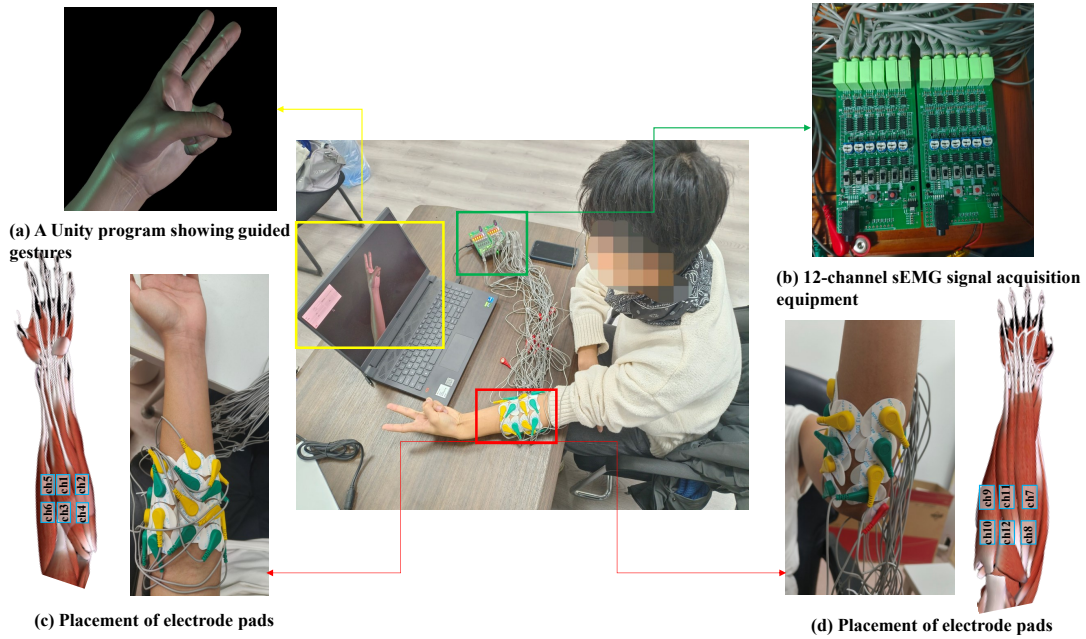


Fig. 2. sEMG data were collected using a 12-channel sensor, covering as much of the forearm muscle groups as possible. The Unity 3D program was used to display guided gestures for participants in data collection.

cluding data collection, signal preprocessing, data set establishment methods and the structure of the model. Section 3 describes the experimental methods and the statistical analysis of the results. Furthermore, our work is discussed in Section 4. Finally, Section 5 concludes this work and outlines future research directions.

2. Methodology

2.1. Inspiration and Model Derivation

2.1.1. Inspiration

Previous theoretical developments have revealed a near-linear relationship between muscle force and corresponding sEMG amplitudes within a specific range [22, 23, 24, 25, 26]. This linear relationship enables simulate intermediate muscle force values by scaling sEMG amplitudes corresponding to maximal finger force within this region. While maximal muscle force output is typically achievable in most hand gestures, the gestures of maximal finger extension and flexion are particularly valuable for our approach. During maximal voluntary contractions (MVC), the forearm muscle groups responsible for these movements engage in isometric contractions, producing maximal force while maintaining a constant muscle length. These MVCs generate discernible sEMG signals [27], facilitating reliable recording and scaling. Although the relationship

between muscle force and sEMG is not perfectly linear at MVC, the sEMG signal recorded during MVC serves as a robust approximation of the muscle’s force output at the upper limit of the linear interval (see Figure 3).

Therefore, to capture sEMG signals representative of

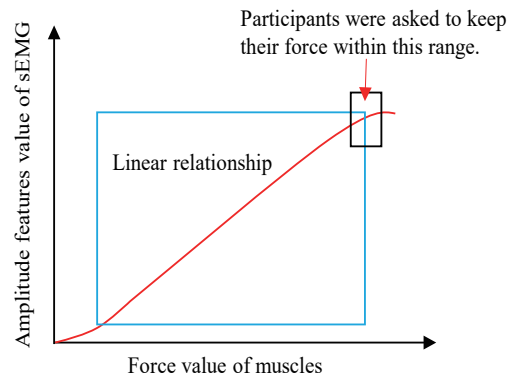


Fig. 3. Relationship between force values of muscles and amplitude features values of sEMG.

maximal muscle force, participants were instructed to perform voluntary maximal finger extension and flexion gestures. This ensures the recorded sEMG signals corresponding to the endpoints of the linear force-sEMG relationship, providing a reliable basis for our estima-

Feature Extraction

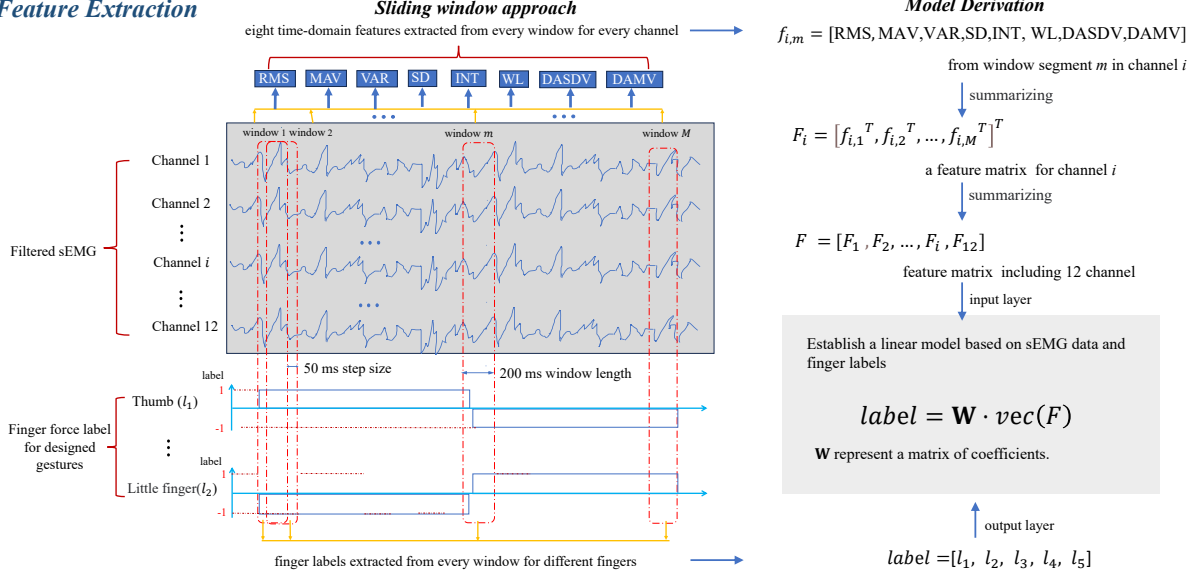


Fig. 4. Feature Extraction. For filtered sEMG signals and finger force labels, a sliding window approach is used to extract eight time-domain features from each window across all channels. Model Derivation. A $12 \times M \times 8$ input matrix is constructed as input matrix, where 12 represents the channels, M represents the number of segments, and 8 corresponds to the time-domain features extracted from each segment. The output matrix contains finger force labels for the five fingers. This setup is used to train models that predict finger force labels based on the extracted input features, enabling the decoding of continuous force and velocity information.

tion method.

2.1.2. Model Derivation

In our study, we established two anchor points based on the MVCs during maximal finger extension and maximal finger flexion (see Figure 1. Part A: Training). Each MVC is associated with specific forearm muscle groups responsible for the different movements. These two extreme conditions of muscle contraction allow us to capture the discernible sEMG signals that closely represent the high end of the muscle force spectrum.

We employed a 12-channel electromyography device to record sEMG signals from the forearm muscles responsible for finger movements in Figure 2.(b). Each muscle group was associated with one or multiple channels. Denoting the sEMG signals from per channel as x_i , we obtained windowed data $w_{i,m}$, with m indexing the window number within the channel i . For each windowed segment $w_{i,m}$, a set of 8 features were extracted, resulting in a feature vector $f_{i,m}$. Detailed features information can be seen in Table 1, the reasons to choose them will be explained in feature extraction. The features extraction process transformed each windowed segment into an 8-dimensional features space, hereby constructing a feature matrix F_i for each channel:

$$F_i = [f_{i,1}^T, f_{i,2}^T, \dots, f_{i,M}^T]^T \quad (2)$$

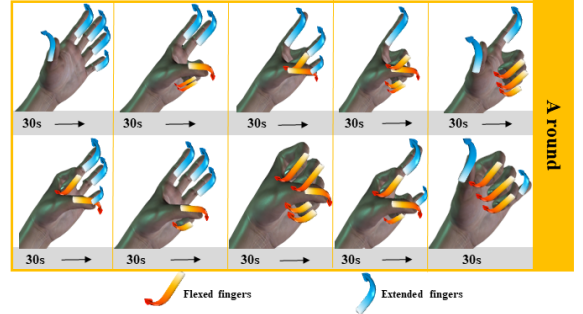


Fig. 5. List of 10 gestures in source gesture set and their force mode, participants hold each gesture for 30 seconds.

where M is the total number of windows extracted from each channel. The feature matrices from all 12 channels were concatenated to form a comprehensive feature tensor F of size $N \times 12 \times M$. The relationship between sEMG data and the finger force labels of forearm muscles is assumed to be an approximate linear model and can be expressed as:

$$\text{label} \approx \mathbf{W} \cdot \vec{F} \quad (3)$$

where \mathbf{W} is a matrix of coefficients, \vec{F} is the vectoriza-

tion of the feature tensor.

$$\vec{F} = [F_1, F_1, \dots, F_{12}] \quad (4)$$

The overall model derivation process can be seen in [Figure 4](#).

Our aim is to employ machine learning-based regression techniques to determine the parameters W . This two-point approach allows us to interpolate the finger force labels values by sEMG activities lying between the two MVCs conditions, thus can predict the finger force output based on [Equation 1](#). It can be used to control the direction and approximate velocity of gestures changes, simplifying computational complexity and eliminating the dependence on kinetic and kinematic sensors.

2.2. sEMG Data Acquisition

2.2.1. Data collection preparation

In our study, twenty able-bodied participants (two females, eighteen males, aged 19.5 ± 1.05 years) provided informed consent to participate in the study protocol. All participants were right-handed and reported no history of neurological or muscular diseases. sEMG signals were recorded from the left forearm of each participant. The study protocol was approved by the ethics review board of Zhengzhou University and adhered to the Declaration of Helsinki and relevant policies in China.

Different gestures are implemented by different finger force patterns. In order to ensure that these gestures include the maximal extension and maximal flexion movements of five fingers, we designed ten gestures as source gesture sets as shown in [Figure 5](#).

The first layer (from left to right) includes the following gestures:

- Maximal Voluntary Extension of all five fingers;
- Maximal Voluntary Extension of the index and middle fingers, with the remaining fingers flexed;
- Maximal Voluntary Flexion of the index and middle fingers, with the remaining fingers extended;
- Maximal Voluntary Extension of the index finger, with the remaining fingers flexed;
- Maximal Voluntary Extension of the thumb and index finger, with the remaining fingers flexed.

The second layer (from left to right) includes the following gestures:

- Maximal Voluntary Flexion of the thumb and index finger, with the remaining fingers extended
- Maximal Voluntary Flexion of the thumb and little finger, with the remaining fingers extended

Table 1: Selected Features with a Monotonic Relationship

Feature name and their abbreviation	Formula
Root Mean Square (RMS)	$\sqrt{\frac{1}{N} \sum_{i=1}^N x_i^2}$
Mean Absolute Value (MAV)	$\frac{1}{N} \sum_{i=1}^N x_i $
Variance (VAR)	$\frac{1}{N-1} \sum_{i=1}^N (x_i - \bar{x})^2$
Standard Deviation (SD)	$\sqrt{\frac{1}{N-1} \sum_{i=1}^N (x_i - \bar{x})^2}$
Integral (INT)	$\sum_{i=1}^N x_i $
Wavelength (WL)	$\sum_{i=1}^{N-1} x_{i+1} - x_i $
Difference Absolute Standard Deviation Value (DASDV)	$\sqrt{\frac{1}{N-1} \sum_{i=1}^{N-1} (x_{i+1} - x_i)^2}$
Difference Absolute Mean Value (DAMV)	$\frac{1}{N-1} \sum_{i=1}^{N-1} x_{i+1} - x_i $

- Maximal Voluntary Flexion of all five fingers;
- Maximal Voluntary Extension of the little and middle fingers, with the remaining fingers flexed;
- Maximal Voluntary Extension of the thumb and little finger, with the remaining fingers flexed

In designing these ten gestures, we considered two key criteria: 1) Comprehensive Coverage: The gestures must include maximum voluntary extension and flexion of all five fingers to capture the full range of finger motion. 2) Real-World Relevance: The gestures should be common and easily performed by participants, such as the “camera gesture,” ensuring comfort and minimizing fatigue during data collection.

2.2.2. Data acquisition process

A 12-channel sEMG acquisition system paired with a PC was used to record sEMG signals at a sampling rate of 1 kHz. Real-time sEMG data was transmitted via a serial port and processed using Python for immediate analysis. Ag/AgCl gel electrodes with a 25 mm spacing were employed to capture the sEMG signals, positioned to cover the entire muscle group of the forearm as comprehensively as possible. Detailed pictures and information regarding the electrode placement are provided in [Figure 2](#).

Participants were seated in a comfortable chair with their left arm placed on a table. They were instructed to perform ten predefined gestures, which were displayed on a monitor screen. Each gesture was held for 30 seconds and counted as one set. Every participant repeated the set of gestures three times, with a five-minute rest interval between each set to minimize muscle fatigue. Previous studies suggested that sEMG amplitude overestimated muscle force when fatigue was present, which

might disrupt the constant linear relationship between muscle force and the sEMG amplitude [22, 26, 28]. This procedure ensured that a complete set of sEMG signals was collected for each gesture.

2.3. Signal Preprocessing and Feature Extraction

After recording the sEMG signals, we combined the three sets of data from each participant to increase the overall dataset, resulting in one comprehensive dataset per person for training purpose.

Since the sEMG signal is extremely weak, it is easy to be disturbed by noise from various sources such as skin, sensors, and the environment. In order to improve the analyzability of the electromyography signal, we must first preprocess it [28]. Firstly, we removed the direct current (DC) component from the 12-channel sEMG data to eliminate any baseline drift [29]. Then, we individually filtered each channel with a 6th order Butterworth bandpass filter from 10 Hz to 450 Hz to remove motion artifacts and high-frequency noise, ensuring that differences in electrode placement do not affect the sEMG signals [29]. A 50 Hz notch filter was also applied to each channel to eliminate power line interference [30]. After filtering, we performed full-wave rectification on the data. For real-time force analysis, low latency and fast response are necessary, and smaller windows can achieve this. Therefore, we processed all data using a sliding window approach (see Figure 4) with a 200ms window length and a 50ms step size [31].

In order to obtain useful information in sEMG and eliminate interfering components, it is necessary to carry out feature extraction. Conventional sEMG signal features include time domain features, frequency domain features and time-frequency domain features [32, 33]. In our two-point approach, the most critical is the use of linear relationship segments, so we extracted eight time-domain amplitude features shown in Table 1 from each of the 12 sEMG channels: Root Mean Square (RMS), Mean Absolute Value (MAV), Variance (VAR), Standard Deviation (SD), Integral (INT), Wavelength (WL), Difference Absolute Standard Deviation (DASDV), and Difference Absolute Mean Value (DAMV). Therefore, the sEMG data mentioned mostly in this paper represents the time-frequency features. While some features share similarities, we found that incorporating a broader set of features significantly enhanced the accuracy of our linear regression model. The model input now consists of a 12×8 matrix, providing a richer representation of the data. Additionally, the model’s adaptive nature allows for automatic adjustment of weights assigned to different input features, further minimizing error.

Table 2: Models and Their Order

Type	Models	Core Formulas	Systems Fit by the Model
Near-linear model	DD (one layer)	$G = WX$ $Y = G \circ C + G$	Second-order system
	LN	$Y = WX$	First-order system
Nonlinear complex model	MLP	$Y = ReLU(WX + b)$	High-order system
	CNN	$C = ReLU[Conv_{2D}(X)]$ $P = Pool(C)$ $Y = ReLU(WP + b)$	High-order system

According to the formulas listed in Table 1, we can infer that the values of these features have a monotonically increasing relationship with the values of the original signal sequence. Therefore, after scaling the original sEMG signals, the scaling relationship will still be preserved in the feature values. And the per-channel feature extraction processing can avoid the differences introduced by variations in electrode patch placement, providing a detailed and robust dataset for analyzing muscle force.

2.4. Specific Model

Based on the Model Derivation section above, we need a model capable of near-linear fitting to meet our linear control requirements. Therefore, we use Dendritic Net (DD) to implement the two-point approach, and use a fully linear network (LN), multi-layer perceptron (MLP) and convolutional neural network (CNN) for performance comparison. The specific neural network diagram is shown in Figure 6 and Table 2.

2.4.1. Near-linear model

DD is a new type of white-box neural network inspired by the dendritic structure of the brain. Our model uses an improved DD, which introduces some special residual connections and contains one layer of DD modules [34, 35]. By adjusting the number of DD modules, the logical expression ability of the algorithm and the order of its fitting system can be effectively adjusted [36, 37, 38]. Its model is capable of fitting up to a second-order system. Its formula can be seen in the Table 2, and the one-layer DD model is capable of fitting up to a second-order system. Its excellent generalization

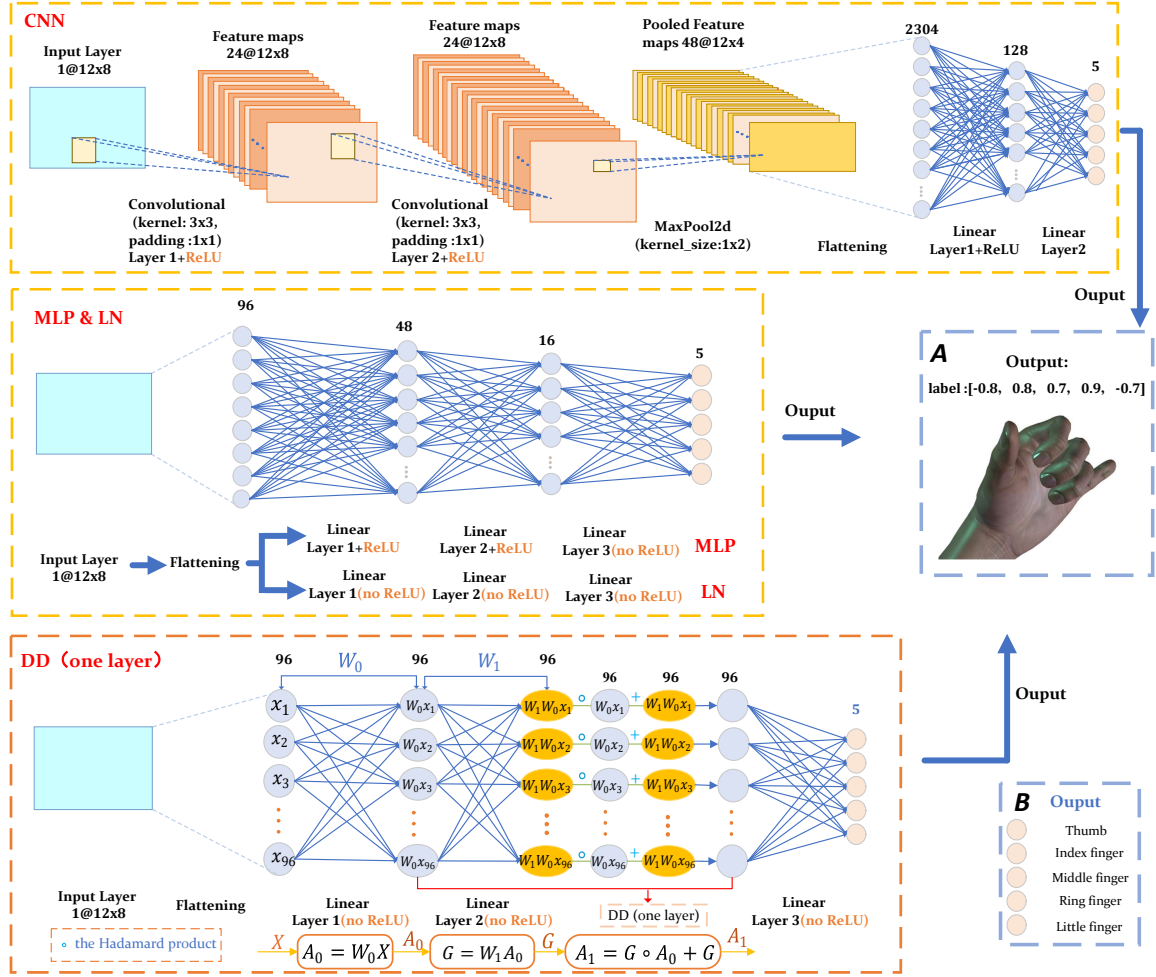


Fig. 6. This figure illustrates the architectures of the CNN, MLP, LN, and DD models used to establish a near-linear model. Each model takes 12 EMG electrode signals as input and generates 5 finger force labels as output, corresponding to the thumb, index, middle, ring, and little fingers. The relationship between the labels and the fingers is shown in B Output, while the Unity virtual control system and the corresponding labels output are displayed in A Output. Additionally, the single-layer DD model is highlighted for its simplicity, consisting of three linear layers without activation functions, which helps maintain a near-linear relationship between the input sEMG signals and the output force labels. Residual connections are used to improve model performance by retaining key information across layers.

ability and low computational complexity are the main reasons for our choice. Detailed structure can be seen in Figure 6. DD (one layer). While the LN represents a network composed entirely of fully connected layers, and the fully connected layers do not have biases.

2.4.2. Nonlinear model

In our study, we selected two nonlinear model representatives, MLP and CNN, whose core formulas are shown in Table 2. The MLP incorporates activation functions such as Sigmoid, ReLU, tanh, etc. (ReLU is used in this study) into the fully connected layers, enabling it to capture complex relationships between inputs and outputs. The CNN uses convolutional kernels

for a certain degree of feature extraction from the inputs, known as convolutional layers, followed by activation functions and pooling for dimensionality reduction [39, 40, 41]. Finally, fully connected layers are used for the output. Both MLP and CNN can implement many relatively complex mappings, but they find it difficult to achieve linear fitting.

2.4.3. Specific models in the experiments

We use a random number seed (random state = 42) to split the unscaled data set, randomly assign one-third as the test set, and the remaining two-thirds as the training set and validation set for ten-fold cross-validation, and shuffle the training data. In order to verify the ability of

the model to interpolate the intermediate value, we also scaled the sEMG data of the partitioned verification set to simulate the sEMG data under different finger force levels. Detailed scaling process can be seen in Figure 7.

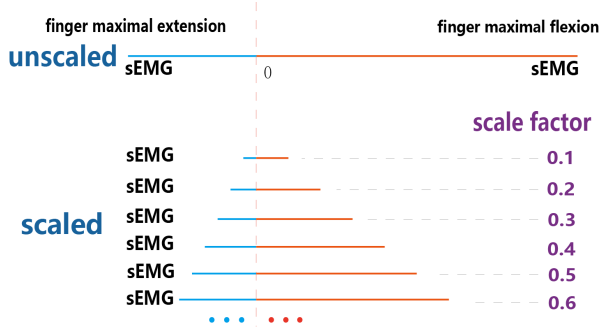


Fig. 7. Scaling process for sEMG amplitudes in different directions (extension and flexion).

The LN in the comparison experiment only uses three fully connected layers, including an input layer and an output layer and a hidden layer, and sets the bias of these fully connected layers to false (see Figure 6. LN). The network structure of MLP is three fully connected layers, and ReLU activation is used after the input layer and hidden layer (see Figure 6. MLP). While CNN uses 2 convolutional layers, 1 max pooling layer and the last 2 fully connected layers, the ReLU activation function is used after the convolutional layer and the first fully connected layer (see Figure 6. CNN). All data are normalized before input, and neither DD nor LN uses activation functions, and none of the four machine learning algorithms uses activation functions at the output layer. The loss function is the mean square error (MSE), using the Adam optimizer with a learning rate of 0.002. Each fold is trained for 15 epochs, and average loss on the validation set is saved. We built unique models for each subject based on their sEMG signal of maximal finger extension and flexion, which will be used for subsequent offline analysis and online experiments.

3. Experiment Results and Analysis

We design offline analysis and online experiments to verify the performance of our model. The flow of offline analysis test is shown in Figure 8. Real-time control of virtual hand experiment is shown in Figure 9.

3.1. Offline Analysis

3.1.1. Force Direction Classification

In our model, the output value represents finger force labels exerted, and the positive and negative represent

Table 3: Offline Analyses Results

Output	Method	Area Under the Curve (AUC)	Standard Error (SE)	Accuracy
L1	DD	0.977887	0.000449	92.22%
	LN	0.929772	0.000804	85.01%
	MLP	0.993835	0.000250	96.63%
	CNN	0.999411	0.000073	99.15%
L2	DD	0.972789	0.000552	90.84%
	LN	0.942453	0.000798	86.07%
	MLP	0.988339	0.000382	94.50%
	CNN	0.998866	0.000113	98.66%
L3	DD	0.982602	0.000398	93.79%
	LN	0.968013	0.000541	91.45%
	MLP	0.992689	0.000272	96.18%
	CNN	0.999116	0.000089	98.85%
L4	DD	0.967460	0.000506	90.94%
	LN	0.919576	0.000812	84.78%
	MLP	0.989969	0.000292	95.55%
	CNN	0.999032	0.000086	98.84%
L5	DD	0.980862	0.000529	93.94%
	LN	0.955773	0.000797	90.28%
	MLP	0.992517	0.000351	96.65%
	CNN	0.998840	0.000131	98.67%

the force direction, that is, whether the finger force is flexion or extension.

We obtain the corresponding five sets of outputs (L1, L2, L3, L4, L5 for five fingers) of the test set for each subject, and merge them to obtain all the outputs of the corresponding five fingers across all subjects. The output value 0 of the model is the threshold for distinguishing the direction of finger force, so 0 is used as the threshold for accuracy calculation. We trained four different machine learning models (DD, LN, MLP and CNN) on the unscaled dataset and evaluated their performance in classifying finger force direction. To verify the model’s performance to learn and decode sEMG information accurately, we conducted offline analysis using the Area Under the Curve (AUC) metric.

After statistical testing, the analysis shown in ($p < 0.001$) Table 3 demonstrates the good performance of the model in the prediction of finger force direction. The AUC values of these models are all over 0.9, very close to 1. It is proved that the output of the models constructed by DD, LN, MLP and CNN can well estimate the direction of finger force.

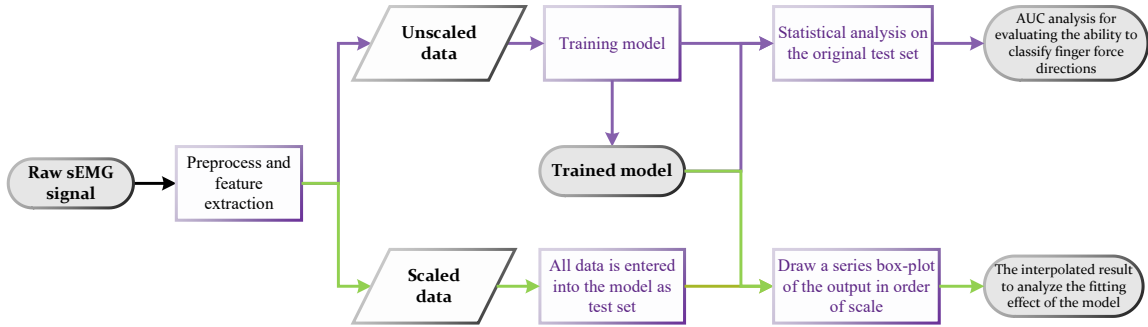


Fig. 8. Offline analysis flow diagram.

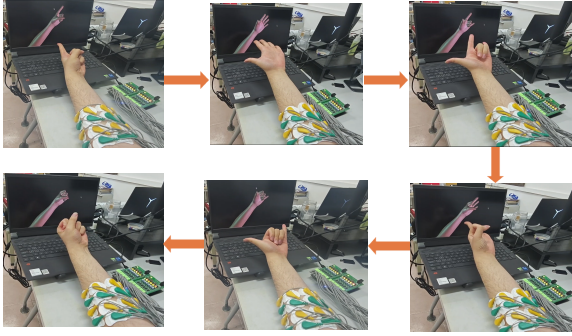


Fig. 9. Real-time control of Unity 3D virtual hands.

3.1.2. Interpolate Force Labels

We further investigate the ability of the model to interpolate intermediate force labels values between two extreme points (-1 and 1). We utilized the previous test datasets. These datasets were scaled to simulate various muscle strength levels, effectively creating test sets for evaluating model fit across the entire force range. Figure 10 showcases the interpolation results for a representative subject, while the rest results of 19 subjects are shown in supplementary material. This analysis allowed us to assess the models' capacity to predict the sEMG-force labels relationship across the entire force spectrum.

Precise control of finger force is crucial for the functionality of prosthetic hands. Previous studies have demonstrated a near-linear relationship between surface electromyography (sEMG) signals and muscle force. This linear relationship is essential for achieving fingers force precise control, as the force generated by the muscles directly dictates the force exerted by the fingers. Only can a linear relationship between sEMG and fin-

ger force enable accurate control, while non-linear relationships make it challenging to achieve. Based on Equation 1, we establish a monotonic and linear relationship between the finger force label and the actual finger force. This suggests that our approach aims for a monotonic and near-linear relationship between sEMG and finger force labels. This characteristic serves as a key performance metric, evaluating the model's capability for intermediate interpolation, a critical aspect of smooth and precise prosthetic hands control.

From the interpolation results of all subjects (see Figure 10), it can be inferred that the models fitted with DD and LN are nearly linear and monotonic, and they complete the supplement of the intermediate value, while MLP and CNN have difficulty in doing so, and have some typical errors, which are unable to make sEMG achieve linear and monotonic control completely for the fingers force label. (For example, (c) and (d) in Figure 10)

Table 4: Statistics Analysis in Fitting Result

Network	DD	LN	MLP	CNN
Error Times	10	8	65	42
Correct rate	90%	92%	35%	58%

We counted all the results of 20 subjects and the results are shown in Table 4. Among the 100 fitting results of each machine learning algorithm, DD made 2 errors and LN made 4 errors. MLP and CNN made 61 errors and 35 errors respectively (see supplementary material).

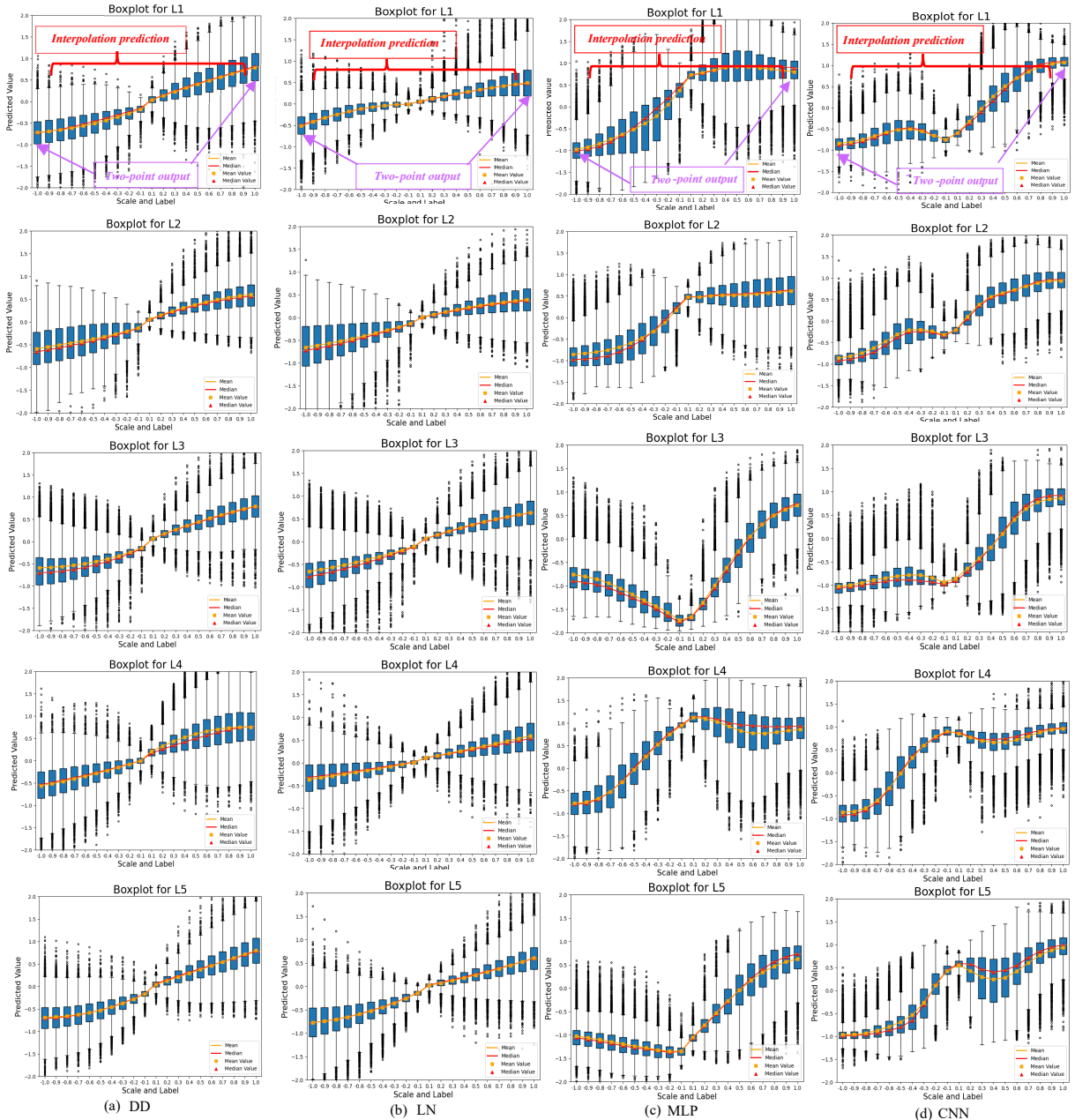


Fig. 10. Visualization of Interpolation Results. The figure displays representative interpolation results from one subject’s data. The abscissa represents the scale factor applied to the sEMG data, where positive values indicate finger flexion, and negative values indicate finger extension. The two ends of each image represent the outputs at the two extreme points, while the middle section shows the interpolated outputs from the models. From L1 to L5, the labels correspond to the pinky to the thumb. Results Analysis. Panels (c) and (d) highlight errors where linear fitting could not be achieved. The failure of these models to accurately interpolate the intermediate values shows the limitations of complex models in maintaining linearity across the data.

3.2. Online Experiments

3.2.1. Sine-Wave Tracking Experiment

To evaluate the practicality for sEMG prosthetics of the model, we designed a sine-wave tracking experi-

ment for online real-time control. Four subjects wore a sEMG acquisition device and were asked to watch a static sine-wave with an amplitude of 1 on screen, and then controlled the direction and size of the finger force

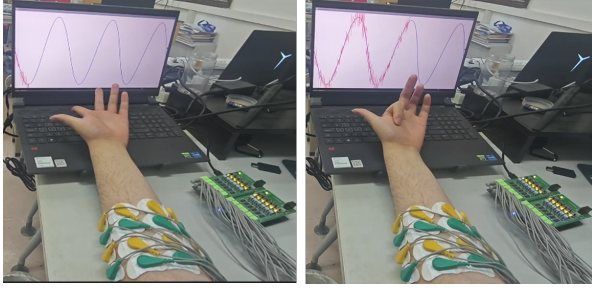


Fig. 11. Sine-wave tracking experiment.

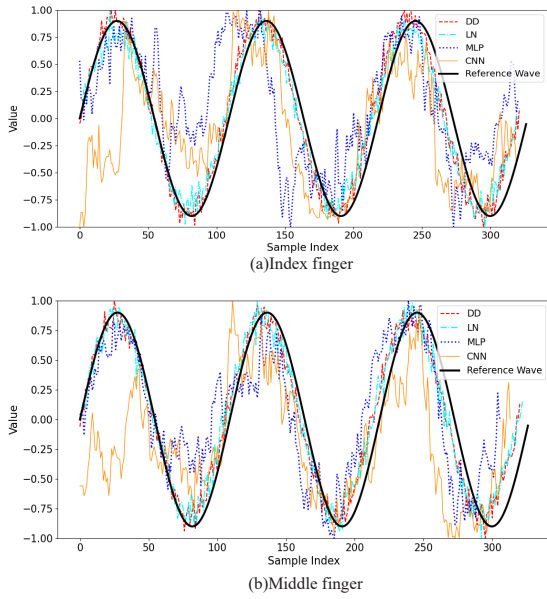


Fig. 12. Waveform diagram of the index and middle finger sine-wave tracking experiment.

at the same time to track the sine-wave on the screen as much as possible. At this time, sEMG would be input into the trained model after real-time processing. The program will draw a curve about sEMG-force labels in real time based on the output of the model. Since the model output value is between 1 and -1, so if the model works well, the curve drawn in real time should match the sine wave.

The experiment was carried out in the form of single-finger control, that is, only the output of the corresponding finger was used to control each time. We selected the index finger and middle finger commonly used in life as the research object. Sine-wave tracking experiment is shown in Figure 11. The waveform diagram of the sine-wave tracking experiment of the index finger and middle finger is shown in Figure 12. By compar-

ing the model-controlled curves to the target sine wave, we can visually assess the models' ability to achieve real-time force control. To accurately evaluate this real-time force control performance, we calculated the average Root-Mean-Square Error (RMSE), Mean Absolute Percentage Error (MAPE), and R-Squared (R^2) for each model. Figure 13 presents the statistical analysis of these metrics, providing a more objective assessment of the models in replicating the desired sinusoidal trajectory accurately.

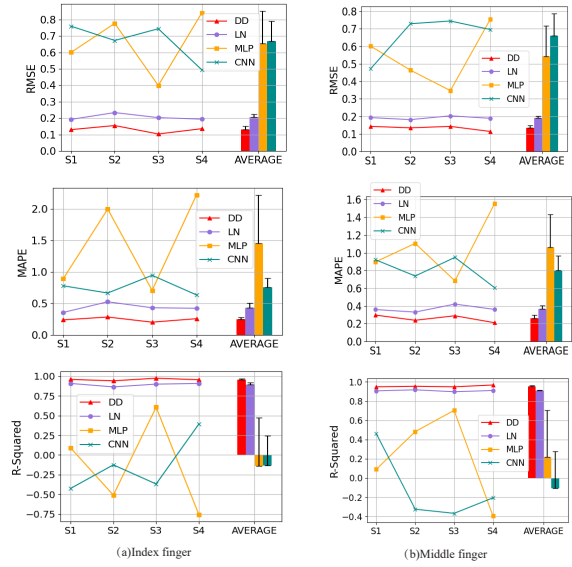


Fig. 13. Performance of RMSE, MAPE, and R-squared metrics in an online sine-wave tracking experiment conducted with four subjects. The error bars represent the standard deviation (SD) across subjects for each metric.

Figure 13 reveals that the majority of RMSE and MAPE values for models built using DD and LN fall within the range of [0.1, 0.2], while R-squared values consistently exceed 0.85. This clustering of data points indicates the high accuracy and excellent data fit of these models. Furthermore, the error bars in Figure 13 demonstrate remarkably low standard deviations for RMSE, MAPE, and R-squared across different subjects for models built using DD and LN, highlighting the stability of their outputs in real-time applications.

In contrast, models utilizing MLP and CNN exhibit significantly larger error bars across subjects, indicating substantial variability and instability in their predictive performance. Notably, for a significant portion of subjects, RMSE values exceed 0.8, MAPE values are greater than 1.6, and R-squared values fall below 1. These findings suggest that real-time force control using

MLP and CNN models presents significant challenges.

Therefore, models employing DD and LN demonstrate superior stability and accuracy across different subjects, making them more suitable for real-time control tasks.

3.2.2. Real-Time Control Demonstration

Building upon the sine-wave tracking experiment, we demonstrated real-time control of all five fingers using our model within the Unity 3D environment. Two videos showcasing this real-time virtual five-finger control are included in the supplementary materials.

These videos highlight the flexibility and continuous nature of gesture estimation achieved with our sEMG-based approach, offering a significant advance over traditional gesture classification methods used in sEMG prosthetic hands control.

To translate real-time sEMG decoding into control signals for the virtual hands model in Unity, we established a relationship between joint angular velocity (ω), joint angular acceleration (α), and finger force labels. First, we utilized the physical relationship between angular velocity and acceleration.

$$\omega = \omega_0 + \alpha \cdot t \quad (5)$$

Where ω_0 represents the initial angular velocity at a given time. Next, we established a linear relationship between angular acceleration and a finger force label value (*label*) based on Equation 1:

$$\alpha = k_\alpha \cdot \text{label} \quad (6)$$

Where k_α is a coefficient used to transform finger force labels into actual angular acceleration. By adjusting the parameter k_α , we can achieve suitable joint angular acceleration for different fingers in real-time (see Figure 1. Part A: Application).

4. Discussion

In this study, we demonstrate an approach without complex kinetic and kinematic parameters to control sEMG prosthetic hands. We use two points (-1 and 1) as extreme label values and corresponding sEMG data to establish a nearly linear model based on sEMG and force labels. We record maximal finger flexion force label as 1 and extension as -1. This model can be used to fit intermediate force label values by scaling extreme sEMG data to decode continuous hand extension and flexion movements with velocity and force information, which eliminates the need for kinetic and kinematic sensors. We conducted offline analysis and online

experiments to verify the effectiveness of our method in accurately predicting force direction, fitting force-myoelectricity relationship, and controlling finger force in real time.

This study involves two research lines. The first thread focuses on controlling a single degree of freedom using sEMG data from two muscle sites, a technique known as “two-site direct control”. Our research extends muscle-based control techniques from single-degree-of-freedom (DOF) to multi-DOF systems with coupled relationships, especially for finger joints. Another research line explores the development of multi-DOF control based on gestures classification and kinetic and kinematic sensors regression mapping. Our research moves beyond traditional discrete gesture classification systems, achieving continuous finger force and gestures estimations. Meanwhile, it also simplifies regression model training dataset acquisition process by eliminating the use of bulky kinetic and kinematic sensors. These result in a more intuitive and user-friendly control system that allows for smoother and more nuanced flexion and extension movements.

In most sEMG prosthesis research, the most common and fundamental upper-limb sEMG control approach is “direct two-site control”, where one sEMG electrode is positioned over the flexor muscle and another over the extensor muscle. The sEMG amplitude from each electrode is processed through rectification and low-pass filtering, and the difference (with thresholding applied) is used to actuate the motor [42].

This study builds upon the strengths of traditional “direct two-site control” research, simplifying prosthesis control by intuitive mapping between muscle activity and prosthesis movement, while further advancing towards more flexible and precise control within the realm of multi-DOF coupled prosthesis control. Specifically, we achieve this by: 1) Expanding the Electromyographic Information Sources. We employ 12 sEMG channels to capture the rich temporal and frequency characteristics of sEMG, thereby offering a significantly broader range of electromyographic information sources for hand joint movements compared to the dual-channel setup used in direct two-site control. 2) Leveraging linear relationships throughout the research process (see Figure 1. Part A and Figure 3). We exploit the linear relationship between sEMG amplitude and muscle force within a specified range to validate our model’s ability to interpolate intermediate values. Additionally, to ensure precise control over finger output force, we establish a near-linear relationship between sEMG data and finger force labels, along with a linear relationship between these labels and the actual finger

forces. This linear proportionality ensures accurate and robust control over finger movement. 3) Existing multi-channel complex pattern recognition methods, which involve multiple sEMG channels for muscle signal decoding, have been shown to achieve high accuracy in multi-DOF joint control. However, their efficiency and real-time performance often fall short due to the complexity of these systems [43]. This study shows a great performance for prosthetic hands real-time control in online experiment and Unity virtual control simulations (see Unity virtual control simulations in supplementary material).

In the main direction of myoelectric interface research, most research is on the classification of gestures through pattern recognition [6, 7, 9]. These related works only focus on the gesture itself and ignore the movement itself. The gestures controlled in this form are limited to some predefined ones, making it difficult to realize complex hand joint movements. Meanwhile, existing research on estimation for hands continuous movements based on neural network model cannot avoid using of other kinetic parameters besides sEMG [17]. This reliance limits their applicability in real-world scenarios where these parameters may not be readily available. In contrast, based on the work of predecessors, this study starts from the sEMG signals of the muscle groups that control finger movement and uses only two points of data to direct map of EMG signals to finger force labels, which can be transferred into actual force easily based on Equation 1. It simplifies the process of decoding continuous finger force from the sEMG signals. This means that in future applications that use sEMG signals for hand movement control, we can eliminate the need of kinetic and kinematic sensors. So complexity of building sEMG prosthetic hands systems can be simplified.

From the beginning of the design of the dataset, our gesture examples included the extension and flexion states of all fingers, and subsequently discarded the sEMG signal when changing the gesture to avoid possible data leakage. The accuracy of the four machine learning methods in finger force direction classification is higher (DD: 92.35%, LN: 87.52%, MLP: 95.90%, CNN: 98.89%, five-finger average), indicating that the two-point method is effective in identifying finger force direction, and they capture the basic information needed for finger movements estimation from sEMG signals. In offline analysis, the near-linear fitting results obtained by the DD and LN models demonstrate their ability to interpolate intermediate the force labels values, which is crucial for accurately controlling the force magnitude and velocity of the prosthetic hands. In contrast, com-

plex models such as MLP and CNN struggle to achieve this because they tend to overfit or exhibit uncontrollable behavior, making them unsuitable for interpolating intermediate values.

We can discuss this in terms of the structure of these networks. First, there are only fully connected layers in LN, and the output is a linear combination of inputs, given an input vector X with weight W , the output Y of LN can be expressed as:

$$Y = WX \quad (7)$$

This linear transformation preserves the monotonic relationship between input and output. If the input sEMG features have a near-linear relationship to the finger force labels, the LN will be able to capture and maintain this relationship, allowing for accurate interpolation of the intermediate force values. Compared with LN, the outputs of the first two layers of MLP are followed by ReLU activation functions. Given the input vector X , the one-layer output Y of an MLP with ReLU activation can be expressed as:

$$Y = ReLU(WX + b) \quad (8)$$

Where W and b are the weight and bias of the layer respectively. The introduction of ReLU functions allows MLP to capture more complex relationships between inputs and outputs, which can fit training data more accurately, but is difficult to interpolate accurately [39, 44] (see Figure 10 and Table 4). In our task, CNN is similar to MLP, although it introduces convolution computation and pooling operation to better capture useful information in the input, it has nonlinear activation function like MLP. We then discuss DD, which combines a linear transformation with a non-linear gating mechanism [34, 37, 40]. In the hidden layer of DD, given the output C of the input layer, the gating signal G :

$$G = W_g \circ C \quad (9)$$

Where W_g is the weight, and then the gating signal G is combined with the residual connection C to obtain the output Y of the DD layer:

$$Y = G \circ C + C \quad (10)$$

There are gating mechanisms and residual connections in DD, which combine linear transformation and non-linear characteristics to preserve the linear relationship between input and output [40], while learning more complex relationships than LN (see Figure 6. DD (one layer)). Regarding the fitting errors shown in the Table 4, theoretically DD and LN should not exhibit such

errors. However, because the VAR values among the eight time-domain amplitude features we selected does not have a strictly linear relationship with the signal sequence values, for example, if the original sequence x_i has a VAR value of V , the VAR value after scaling x_i by 0.7 would be $0.49V$, which is a quadratic relationship. In addition, the reason why the number of errors in DD is slightly larger than that in LN may be that residual connection is introduced in DD we used, which introduces certain nonlinearity, but at the same time can capture more about the relationship between input and output, which is reflected in the better performance (see [Figure 12](#) and [Figure 13](#)) of DD in the sine-wave tracking experiment.

Online experiments further verify the practicality of our method in real-time control scenarios. Sine-wave tracking experiments demonstrate the ability of the DD and LN models to accurately control the direction and magnitude of finger force in real time. Both models achieve low RMSE and MAPE values, as well as high R-squared. Complex models such as MLP and CNN face challenges in real-time force control due to the inability to interpolate intermediate values and the time delays introduced by more complex network structures. These results highlight the importance of model selection in real-time prosthetic control, where simplicity and interpretability are key factors. The Unity virtual control simulations visually demonstrate the exceptional performance of our method for real-time control of prosthetic hands. However, we can clearly observe in the video that the extension movement of the thumb progresses slowly throughout the continuous motion, unlike the flexible flexion and extension movements of the other four fingers. To address this issue, we repeatedly conducted experiments under different conditions with various subjects. The results were similar, indicating that the problem arises due to an improper adjustment of the control angular acceleration parameter k_α . We believe the thumb can achieve the same level of flexibility as the other fingers after fine-tuning this parameter in subsequent experiments.

This primary limitation of this study is the lack of disabled subjects. While previous research suggests similar muscle activation patterns between amputees and non-disabled individuals, further validation with amputee participants is crucial [41]. Additionally, the study does not fully address the coupling effect, where movement of one finger can influence the activation of other fingers [45, 46]. This effect poses a particular challenge for the thumb, which has a wider range of motion and complex movements, further highlighting the need for more sophisticated control strategies in future

research.

Another limitation of this study is that it doesn't cover more complex movements, such as two-finger and three-finger pinching, which require greater degrees of freedom especially for thumb. Current research often relies on complex kinetic and kinematic sensors to achieve these types of movements. Future research could consider exploring sensor-free methods for controlling these complex movements, paving the way for more flexible and user-friendly prosthetic hand systems.

5. Conclusion

In this paper, we present a novel kinetic and kinematic sensor-free approach for controlling sEMG-based prosthetics. This method involves collecting sEMG data at two extreme label points (-1 and 1) to establish a near-linear model that maps sEMG signals to finger force labels. Specifically, maximal finger flexion force is assigned a label of 1, while extension force is labeled as -1. Our approach enables continuous estimation of finger forces and gestures for both single-finger and multi-finger extension and flexion movements. This study demonstrates the effectiveness of this approach in several key areas: 1) High Accuracy in Force Direction Classification: The model effectively learns the relationship between muscle activation and finger force labels, achieving high accuracy in classifying finger flexion and extension directions during offline analysis. 2) Effective Force Labels Interpolation: Monotonic relationships, when combined with near-linear models (DD and LN), effectively interpolate intermediate force labels values, enabling precise control of force magnitude, while complex models with unlimited approximation ability, such as CNN and MLP, have difficulty in inserting the intermediate value due to the inability to control the order of the model. This effective interpolation capability ensures accurate decoding of continuous finger flexion and extension movements. 3) Promising Real-time Control: Through the real-time control of the virtual hand experiment in Unity 3D and the single-finger sine-wave experiment, it has been demonstrated that our method has potential in prosthetic fingers control applications. General, this kinetic and kinematic sensor-free approach simplifies the development of sEMG prosthetics by eliminating the need for complex kinetic and kinematic parameters. By accurately estimating continuous finger forces and gestures using only sEMG data, our method facilitates a more user-friendly and cost-effective approach to prosthetic control, paving the way for future advancements in the field.

References

- [1] D. S. De Oliveira, A. Casolo, T. G. Balshaw, S. Maeo, Lanza, Neural decoding from surface high-density emg signals: influence of anatomy and synchronization on the number of identified motor units, *JOURNAL OF NEURAL ENGINEERING* 19 (4) (2022) 046029. doi:10.1088/1741-2552/ac823d.
- [2] W. Yansheng, L. Shili, C. Zekun, Q. Xiupeng, M. Yongkai, "difference analysis of musculation and estimation of semg-to-force in process of increasing force and decreasing force", *EXPERT SYSTEMS WITH APPLICATIONS* 228 (OCT 15 2023). doi:10.1016/j.eswa.2023.120445.
- [3] X. Sun, X. Zhang, Z. Lu, R. Li, H. Li, T. Zhang, *semg based continuous estimation of wrist joint angle using bp neural network*, 2019 IEEE 9th Annual International Conference on CYBER Technology in Automation, Control, and Intelligent Systems (CYBER) (2019) 221–225. URL <https://api.semanticscholar.org/CorpusID:215815483>
- [4] H. Huang, F. Zhang, L. J. Hargrove, Z. Dou, D. R. Rogers, K. B. Englehart, "continuous locomotion-mode identification for prosthetic legs based on neuromuscular-mechanical fusion", *IEEE TRANSACTIONS ON BIOMEDICAL ENGINEERING* 58 (10, 1) (2011) 2867–2875. doi:10.1109/TBME.2011.2161671.
- [5] D. Bai, S. Yao, J. Yang, P. Yu, S. Chen, C. Ni, Upper arm force semg analysis based on svm, in: 2018 IEEE INTERNATIONAL CONFERENCE ON INTELLIGENCE AND SAFETY FOR ROBOTICS (ISR), UFC; IEEE, 2018, pp. 569–574. doi:10.1109/IISR.2018.8535798.
- [6] K. Kiguchi, Y. Hayashi, An emg-based control for an upper-limb power-assist exoskeleton robot, *IEEE TRANSACTIONS ON SYSTEMS MAN AND CYBERNETICS PART B-CYBERNETICS* 42 (4, SI) (2012) 1064–1071. doi:10.1109/TSMCB.2012.2185843.
- [7] M. Atzori, M. Cognolato, H. Mueller, Deep learning with convolutional neural networks applied to electromyography data: A resource for the classification of movements for prosthetic hands, *FRONTIERS IN NEUROBOTICS* 10 (SEP 7 2016). doi:10.3389/fnbot.2016.00009.
- [8] Z. Wu, H. Niu, D. Li, F. Pu, Y. Fan, A virtual semg prosthetic hand development system based on labview and pci-1710hg a/d card, in: Proceedings of the 2010 3rd International Conference on Biomedical Engineering and Informatics (BMEI 2010), 2010, pp. 1743–5. doi:10.1109/BMEI.2010.5640048.
- [9] U. Côté-Allard, C. L. Fall, A. Drouin, A. Campeau-Lecours, C. Gosselin, K. Glette, F. Laviolette, B. Gosselin, Deep learning for electromyographic hand gesture signal classification using transfer learning, *IEEE Transactions on Neural Systems and Rehabilitation Engineering* 27 (4) (2019) 760–771. doi:10.1109/TNSRE.2019.2896269.
- [10] X. Zhai, B. Jelfs, R. H. M. Chan, C. Tin, Self-recalibrating surface emg pattern recognition for neuroprosthesis control based on convolutional neural network, *FRONTIERS IN NEUROSCIENCE* 11 (JUL 11 2017). doi:10.3389/fnins.2017.00379.
- [11] Y. Hu, Y. Wong, W. Wei, Y. Du, M. Kankanhalli, W. Geng, A novel attention-based hybrid cnn-rn architecture for semg-based gesture recognition, *PLOS ONE* 13 (10) (OCT 30 2018). doi:10.1371/journal.pone.0206049.
- [12] H. Su, W. Qi, Z. Li, Z. Chen, G. Ferrigno, E. De Momi, Deep neural network approach in emg-based force estimation for human-robot interaction, *IEEE Transactions on Artificial Intelligence* 2 (2021) 404–12. doi:10.1109/TAI.2021.3066565.
- [13] G. Liu, L. Wang, J. Wang, A novel energy-motion model for continuous semg decoding: from muscle energy to motor pattern, *JOURNAL OF NEURAL ENGINEERING* 18 (1) (FEB 2021). doi:10.1088/1741-2552/abbece.
- [14] Y. Zheng, X. Hu, Real-time isometric finger extension force estimation based on motor unit discharge information, *JOURNAL OF NEURAL ENGINEERING* 16 (6) (DEC 2019). doi:10.1088/1741-2552/ab2c55.
- [15] F. Zhang, P. Li, Z.-G. Hou, Z. Lu, Y. Chen, Q. Li, M. Tan, semg-based continuous estimation of joint angles of human legs by using bp neural network, *NEUROCOMPUTING* 78 (1, SI) (2012) 139–148. doi:10.1016/j.neucom.2011.05.033.
- [16] Q. Ding, J. Han, X. Zhao, Continuous estimation of human multi-joint angles from semg using a state-space model, *IEEE TRANSACTIONS ON NEURAL SYSTEMS AND REHABILITATION ENGINEERING* 25 (9) (2017) 1518–1528. doi:10.1109/TNSRE.2016.2639527.
- [17] B. Lv, X. Sheng, W. Guo, X. Zhu, H. Ding, Towards finger gestures and force recognition based on wrist electromyography and accelerometers, in: *INTELLIGENT ROBOTICS AND APPLICATIONS, ICIRA 2017, PT I*, 2017, pp. 373–380. doi:10.1007/978-3-319-65289-4_36.
- [18] Y. Chai, K. Liu, C. Li, Z. Sun, L. Jin, T. Shi, A novel method based on long short term memory network and discrete-time zeroing neural algorithm for upper-limb continuous estimation using semg signals, *BIOMEDICAL SIGNAL PROCESSING AND CONTROL* 67 (MAY 2021). doi:10.1016/j.bspc.2021.102416.
- [19] S. Stapornchaisit, Y. Kim, A. Takagi, N. Yoshimura, Y. Koike, Finger angle estimation from array emg system using linear regression model with independent component analysis, *FRONTIERS IN NEUROBOTICS* 13 (SEP 26 2019). doi:10.3389/fnbot.2019.00075.
- [20] C. Chen, Y. Yu, X. Sheng, X. Zhu, Non-invasive analysis of motor unit activation during simultaneous and continuous wrist movements, *IEEE JOURNAL OF BIOMEDICAL AND HEALTH INFORMATICS* 26 (5) (2022) 2106–2115. doi:10.1109/JBHI.2021.3135575.
- [21] J. G. Ngeo, T. Tamei, T. Shibata, Continuous and simultaneous estimation of finger kinematics using inputs from an emg-to-muscle activation model, *JOURNAL OF NEUROENGINEERING AND REHABILITATION* (2014) 122doi:10.1186/1743-0003-11-122.
- [22] J. L. Dideriksen, D. Farina, R. M. Enoka, Influence of fatigue on the simulated relation between the amplitude of the surface electromyogram and muscle force, *PHILOSOPHICAL TRANSACTIONS OF THE ROYAL SOCIETY A-MATHEMATICAL PHYSICAL AND ENGINEERING SCIENCES* (2010) 2765–2781doi:10.1098/rsta.2010.0094.
- [23] J. J. Woods, B. Bigland-Ritchie, Linear and non-linear surface emg/force relationships in human muscles. an anatomical/functional argument for the existence of both., *Am J Phys Med* 62 (6) (1983) 287–299. doi:10.2165/00007256-198401060-00006.
- [24] P. Zhou, W. Rymer, Factors governing the form of the relation between muscle force and the emg: A simulation study, *JOURNAL OF NEUROPHYSIOLOGY* 92 (5) (2004) 2878–2886. doi:10.1152/jn.00367.2004.
- [25] T. J. Roberts, A. M. Gabaldon, Interpreting muscle function from emg: lessons learned from direct measurements of muscle force, *INTEGRATIVE AND COMPARATIVE BIOLOGY* 48 (2008) 312–320. doi:10.1093/icb/icn056.
- [26] H. Kranz, J. F. Cassell, G. F. Inbar, Relation between electromyogram and force in fatigue., *Journal of Applied Physiology* 59 (3) (1985) 821–825. doi:10.2170/jphysiol.35.1101.

- [27] T. Sadamoto, F. Bonde-Petersen, Y. Suzuki, Skeletal muscle tension, flow, pressure, and emg during sustained isometric contractions in humans, *European Journal of Applied Physiology and Occupational Physiology* 51 (3) (1983) 395–408. doi:10.1007/BF00429076.
- [28] R. Merletti, G. L. Cerone, Tutorial. surface emg detection, conditioning and pre-processing: Best practices, *JOURNAL OF ELECTROMYOGRAPHY AND KINESIOLOGY* 54 (OCT 2020). doi:10.1016/j.jelekin.2020.102440.
- [29] C. J. De Luca, L. D. Gilmore, M. Kuznetsov, S. H. Roy, Filtering the surface emg signal: Movement artifact and baseline noise contamination, *JOURNAL OF BIOMECHANICS* 43 (8) (2010) 1573–1579. doi:10.1016/j.jbiomech.2010.01.027.
- [30] J. Piskrowski, Time-efficient removal of power-line noise from emg signals using iir notch filters with non-zero initial conditions, *BIOCYBERNETICS AND BIOMEDICAL ENGINEERING* 33 (3) (2013) 171–178. doi:10.1016/j.bbe.2013.07.006.
- [31] R. N. Khushaba, K. Nazarpour, Decoding hd-emg signals for myoelectric control-how small can the analysis window size be?, *IEEE ROBOTICS AND AUTOMATION LETTERS* 6 (4) (2021) 8569–8574. doi:10.1109/LRA.2021.3111850.
- [32] A. Phinyomark, P. Phukpattaranont, C. Limsakul, Feature reduction and selection for emg signal classification, *EXPERT SYSTEMS WITH APPLICATIONS* 39 (8) (2012) 7420–7431. doi:10.1016/j.eswa.2012.01.102.
- [33] M. Zardoshti-Kermani, B. Wheeler, K. Badie, R. Hashemi, Emg feature evaluation for movement control of upper extremity prostheses, *IEEE Transactions on Rehabilitation Engineering* (1995) 324–333 doi:10.1109/86.481972.
- [34] G. Liu, J. Wang, Eegg: An analytic brain-computer interface algorithm, *IEEE TRANSACTIONS ON NEURAL SYSTEMS AND REHABILITATION ENGINEERING* 30 (2022) 643–655. doi:10.1109/TNSRE.2022.3149654.
- [35] G. Liu, It may be time to perfect the neuron of artificial neural network (2020). doi:10.36227/techrxiv.12477266.v4.
- [36] C. Luo, J. Wang, Q. Miao, Transient current ratio dendrite net for high-resistance connection diagnosis in bldcm, *IEEE TRANSACTIONS ON POWER ELECTRONICS* 39 (4) (2024) 4746–4757. doi:10.1109/TPEL.2024.3356069.
- [37] G. Liu, J. Wang, Dendrite net: A white-box module for classification, regression, and system identification, *IEEE TRANSACTIONS ON CYBERNETICS* 52 (12) (2022) 13774–13787. doi:10.1109/TCYB.2021.3124328.
- [38] G. Liu, J. Wang, A relation spectrum inheriting taylor series: muscle synergy and coupling for hand, *FRONTIERS OF INFORMATION TECHNOLOGY & ELECTRONIC ENGINEERING* 23 (1, SI) (2022) 145–157. doi:10.1631/FITEE.2000578.
- [39] A. Pinkus, Approximation theory of the mlp model in neural networks, *Acta Numerica* 8 (1999) 143–95. doi:10.1017/s0962492900002919.
- [40] G. Liu, Y. Pang, S. Yin, X. Niu, J. Wang, H. Wan, Dendrite net with acceleration module for faster nonlinear mapping and system identification, *MATHEMATICS* 10 (23) (DEC 2022). doi:10.3390/math10234477.
- [41] N. Jiang, H. Rehbaum, I. Vujaklija, B. Graimann, D. Farina, Intuitive, online, simultaneous, and proportional myoelectric control over two degrees-of-freedom in upper limb amputees, *IEEE Trans Neural Syst Rehabil Eng* 22 (3) (2014) 501–510. doi:10.1109/TNSRE.2013.2278411.
- [42] E. Scheme, K. Englehart, Electromyogram pattern recognition for control of powered upper-limb prostheses: State of the art and challenges for clinical use, *JOURNAL OF REHABILITATION RESEARCH AND DEVELOPMENT* 48 (6) (2011) 643–659. doi:10.1682/JRRD.2010.09.0177.
- [43] O. W. Samuel, M. G. Asogbon, Y. Geng, A. H. Al-Timemy, S. Pirbhulal, N. Ji, S. Chen, P. Fang, G. Li, Intelligent emg pattern recognition control method for upper-limb multifunctional prostheses: Advances, current challenges, and future prospects, *IEEE ACCESS* 7 (2019) 10150–10165. doi:10.1109/ACCESS.2019.2891350.
- [44] D. Yarotsky, Error bounds for approximations with deep relu networks, *NEURAL NETWORKS* 94 (2017) 103–114. doi:10.1016/j.neunet.2017.07.002.
- [45] C. E. Lang, M. H. Schieber, Human finger independence: limitations due to passive mechanical coupling versus active neuromuscular control., *Journal of Neurophysiology* 92 (5) (2004) 2802. doi:10.1152/jn.00480.2004.
- [46] H. R. Charlotte, M. H. Schieber, Quantifying the independence of human finger movements: comparisons of digits, hands, and movement frequencies., *Journal of Neuroscience* 20 (22) (2000) 8542–8550. doi:10.1002/1097-4695(20001115)45:3<185::AID-NEU6>3.0.CO;2-G.